European Journal of Pharmaceutics and Biopharmaceutics 134 (2019) 178–184

Contents lists available at ScienceDirect

European Journal of Pharmaceutics and Biopharmaceutics

journal homepage: www.elsevier.com/locate/ejpb

Research paper

Hydroxycamptothecin nanoparticles based on poly/oligo (ethylene glycol): Architecture effects of nanocarriers on antitumor efficacy

Yifei Guo[a], Ting Wang[a,b], Hanhong Qiu[a], Meihua Han[a], Zhengqi Dong[a,*], Xiangtao Wang[a,*], Yanhong Wang[b,*]

[a] Institute of Medicinal Plant Development, Chinese Academy of Medical Sciences & Peking Union Medical College, No. 151, Malianwa North Road, Haidian District, Beijing 100193, China
[b] School of Pharmacy, Heilongjiang University of Chinese Medicine, No. 24, Heping Road, Xiangfang District, Harbin 150040, China

ARTICLE INFO

Keywords:
Influence of architecture
Steric hindrance
HCPT nanoparticles
Antitumor efficacy

ABSTRACT

Nanoparticles decorated with hydrophilic PEG chains had been emerged as effective drug delivery system due to their biocompatibility and biodegradability, while, the influence of their architecture on antitumor efficacy remained challenging. In this study, the linear poly(ethylene glycol) (PEG_{45}), brush oligo(triethylene glycol) (TEG_{10}), and oligo(ethylene glycol) dendron (G2), which showed the similar molar mass but different architecture, were utilized as nanocarriers to prepare 10-hydroxycamptothecin (HCPT) nanoparticles. It was found that all of three HCPT NPs (PEG_{45} NPs, TEG_{10} NPs, and G2 NPs) presented similar DLCs (~60%), zeta potentials (−13 to −16 mv), and stabilities, meanwhile, the particle sizes, morphologies, release profiles, and anticancer efficacies were affected by the architecture of nanocarriers. Changing the architecture from linear, brush to dendron, the mean particles diameter was decreased from 240 to 170 nm, the sustained releases were elongated from 5 to 9 days. More importantly, the cytotoxicity of G2 NPs based on OEG dendron was enhanced significant comparing with linear PEG_{45} NPs, the IC_{50} was decreased almost 10.1-fold ($p < 0.01$). Besides, the tumor inhibition rate of G2 NPs was 1.7-fold higher than PEG_{45} NPs, showing significantly optimized antitumor efficacy *in vivo*. These results suggested the architecture of nanocarriers could affect the antitumor activity, due to the steric hindrance of nanocarriers influence the morphologies of HCPT-loaded nanoparticles.

1. Introduction

Nanoscale drug delivery system (NDDS) has emerged as a promising strategy to enhance the antitumor efficacy of hydrophobic drugs by improving the solubility and passive targeting effects [1–6]. Nonetheless, the clinical applications of NDDS is still limited due to the unsatisfied antitumor efficacy, severe side effects [7,8]. To overcome these defects, various biomaterials have been optimized and utilized as the nanocarriers [9], poly(ethylene glycol) (PEG) as the safe and biocompatible material are studied broadly and have been approved by FDA [10–12], several nanodrugs based on PEG have been utilized in clinic [13].

Based on the influence of nanocarriers' architecture on the cellular uptake and antitumor activity, branched polymers have been explored as the nanocarriers for drug delivery owing to their unique structure [14–18]. Those NDDSs applying branched polymers as nanocarriers showed optimized performance in drug-loading content, stability *in vitro*, releasing, and cellular uptake efficacy than relative linear structures [19–21]. Dendrimers [22–25], Janus dendrimers [26,27], star-shape polymers [28,29], hybrid linear-dendritic copolymers [30,31], and hyperbranched polymers [32,33], have been developed as the nanocarriers to encapsulate anticancer drugs, and these branched systems emerge the good antitumor activity due to their narrow disperse nature and large number of peripheral functional groups [34]. The delivery efficacy of branched polymers, including poly-lysine, polyethyleneimine, poly(β-amino esters) (HPAE)-containing polymers and so on, are found better than their linear counterparts [35,36].

Combining the advantages of branched structure and PEG chains, several polymers containing linear/branched PEG chains are researched as nanocarriers to encapsulate DOX, HCPT, PTX, all these NDDSs exist good drug-loading capacity, controlling release manners, and longer blood circulation [37–39]. While, these related studies mainly focus on applying linear/branched PEGylated nanocarriers to promote the antitumor efficacy, it is difficult to conclude how the architecture of nanocarriers affect the antitumor efficacy due to these nanocarriers presented different structure. Furthermore, few of research study the

* Corresponding authors.
E-mail addresses: ffguo@163.com (Y. Guo), xtaowang@163.com (X. Wang).

https://doi.org/10.1016/j.ejpb.2018.12.003
Received 9 August 2018; Received in revised form 14 November 2018; Accepted 4 December 2018
Available online 05 December 2018

effects of linear/branched PEG chains in these nanocarriers on antitumor efficacy, because it is difficult to prepare drug-loaded nanoparticles only utilizing PEG chains. Therefore, it is impossible to obtain the information how the architecture of PEG affect the antitumor efficacy based on these previous research.

To explore and exploit the desired architecture of nanocarriers in the presence of antitumor efficacy, in this study, the effect of architecture of PEG are studied based on these nanocarriers presenting the similar molar mass but different architecture. Therefore, linear poly (ethylene glycol) (PEG_{45}), brush poly(triethylene glycol) (TEG_{10}), and oligo(ethylene glycol) dendron (G2) were utilized as nanocarriers to prepare 10-hydroxycamptothecin (HCPT)-loaded nanoparticles by solvent exchange method. The particle sizes, morphologies, stabilities, and release profiles were studied. The antitumor activities, biodistributions, and systemic toxicities were estimated at the same time.

2. Materials and methods

2.1. Materials

Hydroxycamptothecin (HCPT) was purchased from Melone Pharmaceutical Co., Ltd. (Dalian, China). HCPT injection was brought from Shenzhen Main Luck Pharmaceuticals Inc. (Shenzhen, China). Acetonitrile were received from Fisher Scientific (USA) for HPLC analysis. Dimethyl formamide (DMF), Dimethyl sulfoxide (DMSO), and normal saline were obtained from Merck. Dialysis bag with MWCO 14000 Da was purchased from Spectrapor (USA). Other reagents and solvents were of analytical grade and used without further purification.

2.2. Animals and cell line

The 4T1 cell line (murine breast cancer) derived from National Infrastructure of Cell Line Resource (Beijing, China) and cultured in RPMI-1640 medium supplemented with 10% fetal bovine serum and 100 units mL^{-1} penicillin G and streptomycin in a humidified 5% CO_2 atmosphere at 37 °C.

BALB/c mice (20 ± 2 g) and rats (200 ± 20 g) were purchased from Vital River Laboratory Animal Technology Co., Ltd (Beijing, China). All the animals were left on SPF conditions, standard diet of food and water ad libitum for 1 week. All experimental procedures were performed in line with the Guidelines and Policies for Ethical and Regulatory for Animal Experiments and approved by the Animal Ethics Committee of Peking Union Medical College (Beijing, China).

2.3. Encapsulation of HCPT by nanocarriers

Ultrasonication-dialysis strategy was applied to prepare HCPT-loaded nanoparticles (HCPT NPs). 8 mg HCPT and 4 mg nanocarriers (PEG_{45}, TEG_{10}, and G2) were dissolved in 1 mL DMF to form organic solution, subsequently injected into MiliQ water (5 mL) under ultrasonication for 10 min. After dialyzed (MWCO 14000) against MiliQ water (4 × 1 L), the drug-loaded nanoparticles were obtained, and then the concentration of HCPT was evaluated via UV-HPLC (UltiMate3000, DIONEX) at 384 nm on a Thermo (4.60 mm × 250 mm, 5 μm) with acetonitrile:water containing 0.1% acetic acid (25:75, v/v). The calibration curve ($y = 1.7874x + 0.1561$, $R^2 = 0.9999$) was generated on C_{18} column, 1.0 mL min^{-1} of flow rate, and 20 μL of the sample injection volume. The drug-loading content (DLC) was calculated as follow.

$$DLC = (\text{weight of loaded drug/weight of drug} - \text{loaded NPs}) \times 100\%$$

2.4. Particle size and morphology experiments

The HCPT NPs was detected by DLS and SEM. The particle size, size distribution, and zeta potential were characterized by Zetasizer Nano-ZS analyzer (Malvern Instruments, UK). Experiments were performed in triplicates. The diluted sample (0.1 mg mL^{-1}) were placed on carbon-matrix, sputter-coated with a conductive layer of gold-palladium (Au/Pd) for 1 min, and then the SEM samples were obtained.

2.5. Stability study

HCPT NPs were storage at 4 and 25 °C for 14 days, the particles sizes were measured at the 0, 2, 7, and 14 days by dynamic light scattering. Besides, HCPT NPs were incubated with 5% glucose solution and plasma at 37 °C, the particle sizes were measured at the 0, 2, 12, and 24 h by dynamic light scattering.

2.6. Release profiles

The HCPT accumulative release measurements were conducted by the dialysis method at 37 °C. In typical experiment, HCPT injection, 2 mL of HCPT NPs solution were added into a dialysis membrane (MWCO 14000 Da), then immersed in 50 mL of PBS solution containing 0.5% SDS at pH 7.4 with continuous magnetic stirring at 100 rpm. At different time intervals, 5 mL external solution was taken out and an equal volume of fresh PBS solution was added, the external solution was analyzed by UV-HPLC at 384 nm.

2.7. Cytotoxicity of HCPT NPs

The HCPT NRs were incubated with the 2% (w/v) RBC suspension at 37 °C for 5 h with different concentrations. Then the RBCs were removed by centrifugation, 150 μL of the supernatant was measured at 540 nm using a microplate reader (Versamax Tunable Microplate Reader). The results were expressed with the assumption that deionized water causes 100% hemolysis and 5% glucose solution 0% hemolysis. The experiments were conducted in triplicate, and the data were shown as the mean values plus standard deviation (± SD).

Murine breast cancer cell line was chosen for MTT assay. 4T1 cells were cultured with RPMI-1640 medium containing with 10% fetal calf serum, 100 units mL^{-1} penicillin G, and streptomycin at 37 °C with 5% CO_2, all cells (1×10^4 cells per well) were seeded in 96-well plates. Before treated with HCPT samples, the cells were incubated for 48 h, then the cultural medium was changed to fresh RPMI-1640. After treated with various formulations and cultured for further 48 h, 20 μL MTT solution (5 mg mL^{-1} in PBS) were added to each well and incubated for 4 h. Subsequently, the medium was removed and 200 μL DMSO was added into each well to dissolve the blue formazan crystals, and the absorbance was measured at 570 nm. The cell inhibition rate was calculated as follows. Cell inhibition = $(1 - OD_{treated}/OD_{control}) \times 100\%$, where $OD_{treated}$ was the value treated by the nanoparticles, $OD_{control}$ was the value treated by the culture medium.

2.8. In vivo anticancer studies

The 5–6 week BALB/c mice (18–22 g) were injected with 5×10^6 4T1 murine breast cancer cells into the same region of each mouse. After reaching a tumor volume of about 100 mm^3, mice were randomly divided into 5 groups (n = 10), and treated separately with 0.2 mL of normal saline (as control), HCPT injection (positive group), HCPT NPs (test groups) via intravenous (i.v.) administration every 2 days for 6 times, which the injected concentrations were equivalent to 3 mg Kg^{-1} HCPT. All the mice were injected every 2 days for 6 times, tumor volume was measured daily with a caliper and calculated as: tumor volume (mm^3) = 0.5 × length (mm) × width $(mm)^2$. After sacrificed, tumors and main organs were excised and weighed. The inhibition rate (IR) of the tumor was calculated as follows.

IR = (1 − mean tumor weight of treatment group / mean tumor weight of control group) × 100%.

2.9. Biodistribution evaluation

The tissues and main organs were collected, washed, accurately weighed, and homogenized with normal saline solution (0.9% NaCl). HPLC with fluorescence detector (excitation/emission wavelengths 375/435 nm) was utilized to detect the actual HCPT concentration, which was performed on a Thermo C_{18} column with acetonitrile/water containing 0.1% acetic acid (30/70, v/v) as eluent. The calibration curves were generated with a flow rate of 1.0 mL min^{-1} and the sample injection volume of 20 μL.

2.10. Statistical analysis

All experiments were conducted at least in triplicate (> 3 independent experiment). Data were presented as the mean values ± SD. Comparison between groups was estimated by one-way analysis of variance (ANOVA) (SPSS 19.0, USA), $P < 0.05$ indicated statistical significance.

3. Results and discussion

3.1. HCPT-loaded nanoparticles

As the analogue of PEG, linear poly(ethylene glycol) (PEG_{45}, Mw = 2000), brush poly(triethylene glycol) (TEG_{10}, Mw = 2460) [40], and oligo(ethylene glycol) dendron (G2, Mw = 2436) [41], were applied as the nanocarriers with similar molar mass but different architecture, hydroxycamptothecin (HCPT)-loaded nanoparticles (HCPT NPs) were prepared according to our previous papers (Fig. 1) [42]. HCPT (8 mg) and nanocarriers (4 mg) were added into DMF to form the organic solutions, subsequently was injected into the MiliQ water under ultrasonication, the PEG_{45} NPs, TEG_{10} NPs, and G2 NPs were obtained after dialysis against distilled water. All of these HCPT NPs presented similar DLCs (~60%), particle size distributions (~0.10, Fig. 2a), and zeta potentials (−13 to −16 mV) (Table 1).

However, these three HCPT NPs existed different particle size and morphology. The hydrodynamic diameter was 240.1, 194.4, and 173.6 nm for PEG_{45} NPs, TEG_{10} NPs, and G2 NPs separately. Besides, morphologies of the HCPT NPs were investigated by SEM, nanorods and nanospheres were shown for PEG_{45} NPs (Fig. 2b) and TEG_{10} NPs (Fig. 2c), and linear PEG_{45} triggered more nanospheres than brush TEG_{10}, meanwhile, for G2 NPs, only nanorods were presented (Fig. 2d). It seemed that the architecture of nanocarriers could affect the hydrodynamic diameter and the shape of drug-loaded nanoparticles, the ratio of nanorods was enhanced with increasing the branched degree of nanocarriers. The similar phenomenon was reported in our previous papers, and could be attributed to the steric hindrance of nanocarriers inducing to form non-spherical nanocrystals [43].

3.2. Measurement of stability

HCPT NPs existed good storage stability at 4 and 25 °C (Fig. 3a and b), the particle sizes were maintained after 14 days. The stabilities of HCPT NPs in different medium were evaluated by DLS, and the hydrodynamic diameter was recorded at different time. After incubated 24 h, the mean diameter of all HCPT NPs were maintained in 5% glucose solution (Fig. 3c) and plasma (Fig. 3d), showing no significant difference ($p > 0.05$) when compared with their original values. These results suggested that these HCPT-loaded nanoparticles possessed good stabilities and met the requirements of animal experiments *in vivo,* on account of the peripheral hydrophilic shells hindered the aggregation of particles.

3.3. Cumulative release study

To evaluate the release profiles of HCPT NPs, HCPT injection was utilized as the control under the similar conditions (Fig. 4). For free HCPT, complete diffusion was found to occur within 4 h due to the carboxylate HCPT in injection was water soluble. Meanwhile, all of these HCPT NPs showed the sustained release behaviors for several days. The significant different release properties could be explained by the structure of HCPT nanoparticles, the hydrophilic shell of drug-loaded nanoparticles might slow the diffusion of HCPT from inside of nanoparticles to outside medium. Although all the nanoparticles

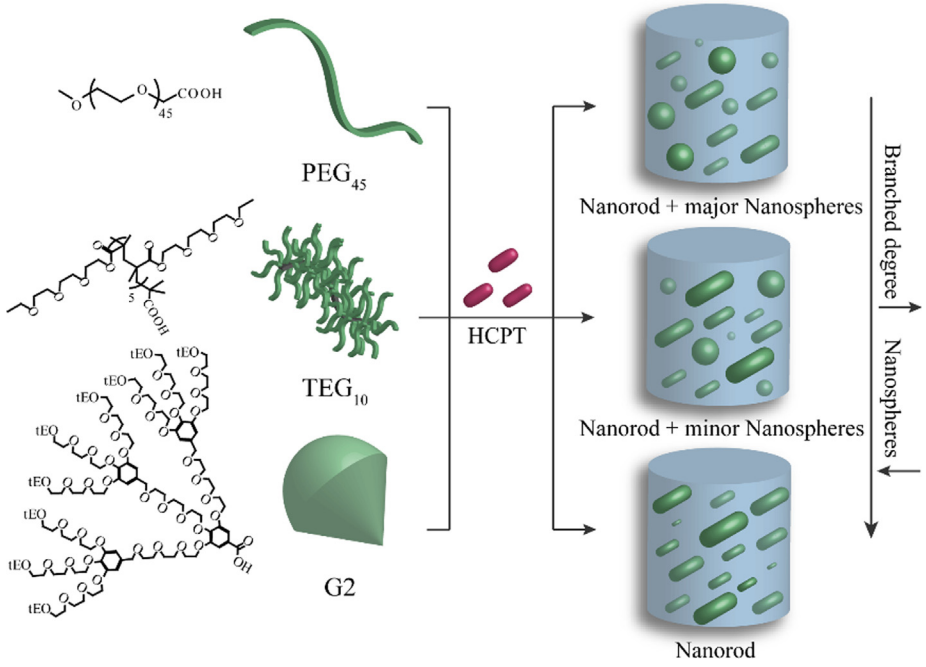

Fig. 1. The structure of three nanocarriers and the HCPT nanoparticles preparing procedure.

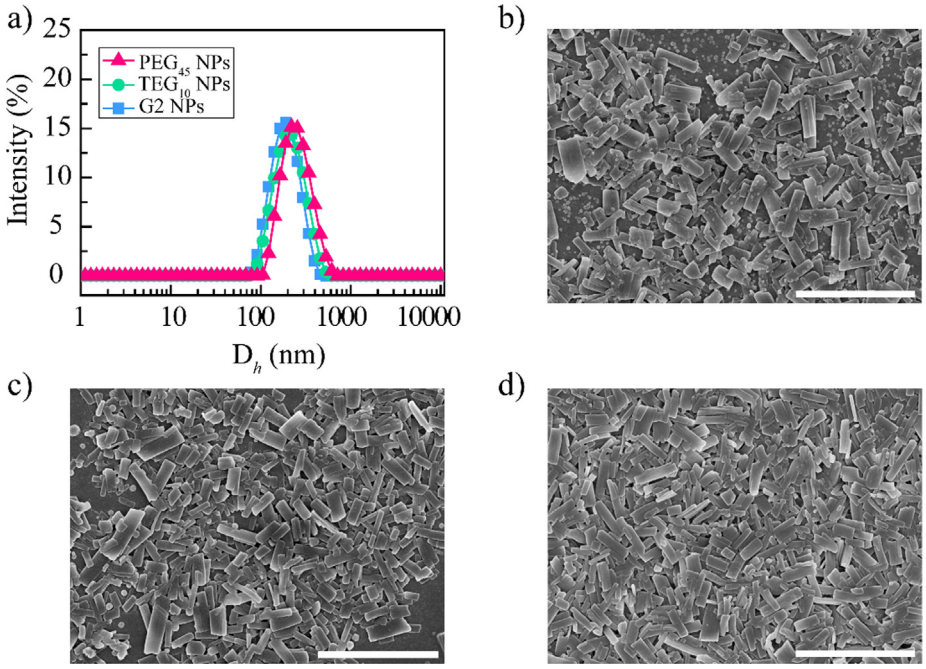

Fig. 2. Particle size distribution curves of HCPT NPs (a), SEM images of PEG_{45} NPs (b), TEG_{10} NPs (c), and G2 NPs (d). Scale bar: 1 μm.

Table 1
Results of different HCPT nanoparticles.

Sample	DLC[a]	D_h (nm)[b]	PDI	ζ (mv)[c]
PEG_{45} NPs	61.1 ± 5.4	240.1 ± 7.1	0.09 ± 0.01	−16.1 ± 0. 2
TEG_{10} NPs	63.2 ± 4.8	194.4 ± 1.0	0.12 ± 0.02	−13.9 ± 0.4
G2 NPs	61.2 ± 3.8	173.6 ± 4.3	0.11 ± 0.04	−15.5 ± 0.5

[a] Detected by UV-HPLC.
[b] Hydrodynamic diameter.
[c] Zeta potential.

showed similar sustained release, the specific process is different. Briefly, the sustained release for 5, 7, and 9 days was measured for PEG_{45} NPs, TEG_{10} NPs, and G2 NPs correspondingly, G2 NPs presented slowest release kinetics. This phenomenon could be explained by the influence of architecture, which increased the rigidity of the hydrophilic shell and extended the release of HCPT due to the steric hindrance.

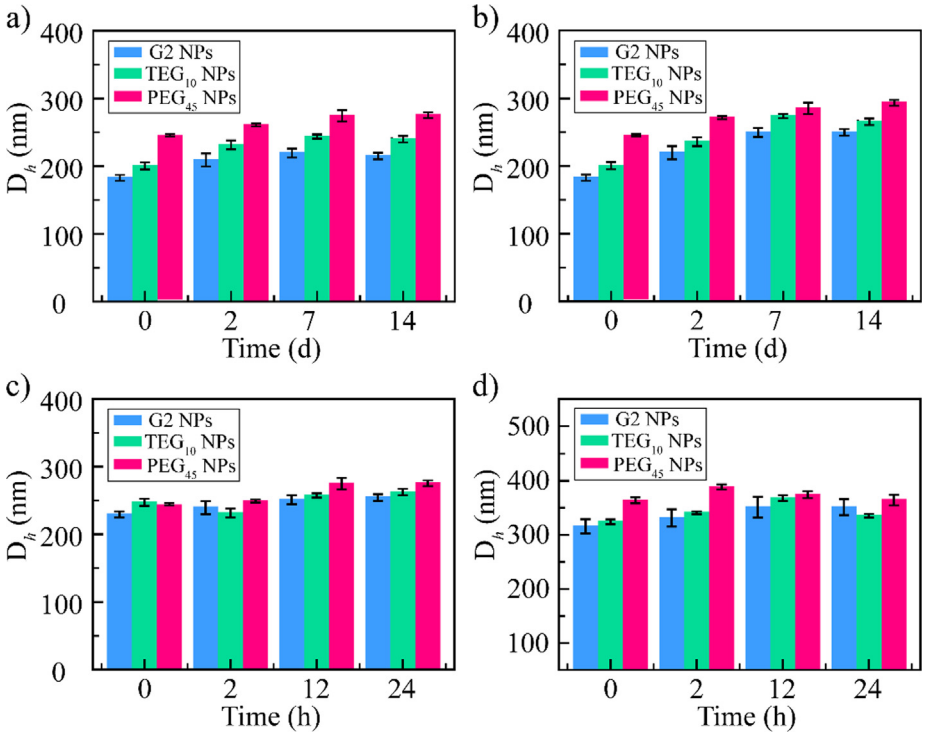

Fig. 3. Particle sizes of the HCPT NPs in aqueous solution at 4 °C (a) and 25 °C (b), in 5% glucose solution (c) and plasma (d) at 37 °C.

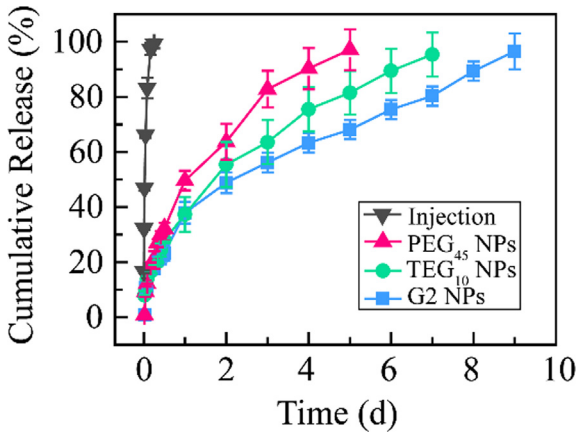

Fig. 4. HCPT cumulative release curves in PBS solution containing 0.5% SDS (pH 7.4) at 37 °C within 9 day (n = 3).

3.4. In vitro cytotoxicity

The hemocompatibility of the three HCPT nanoparticles were estimated to study their toxicity to red blood cells. After incubation with RBC suspension for 5 h, the hemolysis rates were below 3% even if the concentration of HCPT was 10 mg mL^{-1}. Based on these results, it seemed that all of these HCPT NPs didn't exist RBC membrane related toxicity and could be suitable for vein administration.

4T1 breast cancer cell line was selected as the model to estimate the antitumor efficacy of HCPT NPs *in vitro* (Fig. 5). Nanocarriers didn't exhibit cytotoxicity, the cell inhibition rates were below 10% even at the concentration of 100 μg mL^{-1}. However, drug-loaded nanoparticles showed the significantly promoted cytotoxicity, and the inhibition rate existed time-dependent and dose-dependent manners. After incubating for 24 h, all these HCPT NPs showed the cytotoxicity and the IC_{50} was 17.6, 10.5, 8.3, and 3.8 μg mL^{-1} (HCPT equivalent concentration) for HCPT injection, PEG_{45} NPs, TEG_{10} NPs, and G2 NPs respectively (Fig. 5). Prolonging the incubation time from 24 to 48 h, the IC_{50} value for free HCPT, PEG_{45} NPs, TEG_{10} NPs, and G2 NPs was 9.05, 5.41, 3.45, and 0.53 μg mL^{-1} respectively. All of nanoparticles existed a higher cytotoxicity effect comparing with injection ($p < 0.05$). These results indicated more HCPT nanoparticles was uptake by 4T1 cells via the facilitated endocytosis transport, while, passive diffusion was the main route of free HCPT to cross the cell membrane. Besides, three HCPT NPs exerted different cytotoxicity, from PEG_{45} to G2, the cytotoxicity was enhanced significantly, after incubation for 48 h, the IC_{50} value of G2 NPs was decreased approximately 10.1-fold than PEG_{45} NPs ($p < 0.01$) and 6.5-fold than TEG_{10} NPs ($p < 0.01$). It was reported that the cytotoxicity of HCPT NPs was related with the shape of HCPT NPs, nanoparticles with rod-like shape showed the better antitumor efficacy than nanospheres due to the different cellular uptake mechanism [44]. Based on different nanocarriers, three HCPT NPs presented different morphologies, from linear PEG to branched G2, the ratio of nanorods was enhanced with increasing the branched degree of nanocarriers, and therefore, G2 NPs exhibited the best antitumor activity against 4T1 cells.

3.5. In vivo antitumor efficacy

To estimate antitumor efficacy of HCPT NPs, these samples were administrated into BALB/c mice bearing 4T1 tumors with the concentrations were equivalent to 3 mg kg^{-1} HCPT. Mice were randomly divided into 5 groups and administrated with formulations every 2 days for 6 times, tumor volume were measured at the same time (Fig. 6). All tumor volume showed time-relative increasing, the tumor sizes were enlarged by 21.8-fold, 12.6-fold, 10.2-fold, 7.4-fold, and 3.1-fold for blank, positive, PEG_{45} NPs, TEG_{10} NPs, and G2 NPs groups correspondingly (Fig. 6a). Comparing with saline control group, injection group possessed moderate antitumor efficacy, meanwhile, HCPT NPs produced higher antitumor activity than HCPT injection group ($p < 0.05$ for PEG_{45} NPs, $p < 0.01$ for TEG_{10} NPs and G2 NPs). Furthermore, it was found that antitumor activity of these HCPT NPs was influenced by the branched degree of nanocarriers, G2 NPs emerged the best antitumor activity ($p < 0.01$, *vs.* PEG_{45} NPs).

Based on the average weights of the tumors, the inhibition rates were calculated which further indicated the superior tumor inhibition activity of nanoparticles (Fig. 6b). The average weight of the tumor was 0.91, 0.66, 0.58, 0.40, and 0.21 g for blank, positive, PEG_{45} NPs, TEG_{10} NPs, and G2 NPs groups, the relative tumor inhibition rate was 37.6%, 45.6%, 55.6%, and 77.1% for positive, PEG_{45} NPs, TEG_{10} NPs, and G2 NPs groups, respectively. The promoted tumor inhibition rate of HCPT nanoparticles was attributed to longer blood circulation [45,46], higher accumulation in tumor tissue via EPR effect [47,48], and higher cell endocytosis efficacy [49]. It was confirmed that the architecture of nanocarriers could affect the antitumor activity, due to the self-assembly behavior was affected by the branched structure of nanocarriers.

3.6. Biodistribution measurement

The concentrations of HCPT in tumor and major organs were evaluated after sacrificed (Fig. 7). Comparing with HCPT injection, all nanoparticles existed better tumor accumulation, the biodistribution were enhanced significantly, on account of the nanoparticles could be passive targeted to tumor tissue via EPR effects. Moreover, G2 NPs showed the best tumor accumulation than other HCPT NPs, due to the cellular uptake was affected by the morphology of nanoparticle. Beside tumor tissue, HCPT nanoparticles were also mainly distributed in liver and kidney that was the common phenomenon, due to the phagocytosis

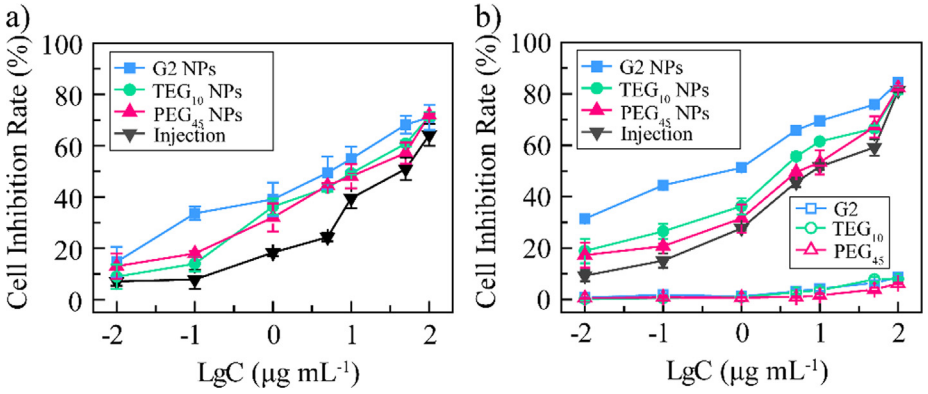

Fig. 5. Cytotoxicity of HCPT NPs *in vitro*. Breast tumor cell 4T1 incubated with HCPT injection and nanoparticles for 24 h (a) and 48 h (b) (n = 5).

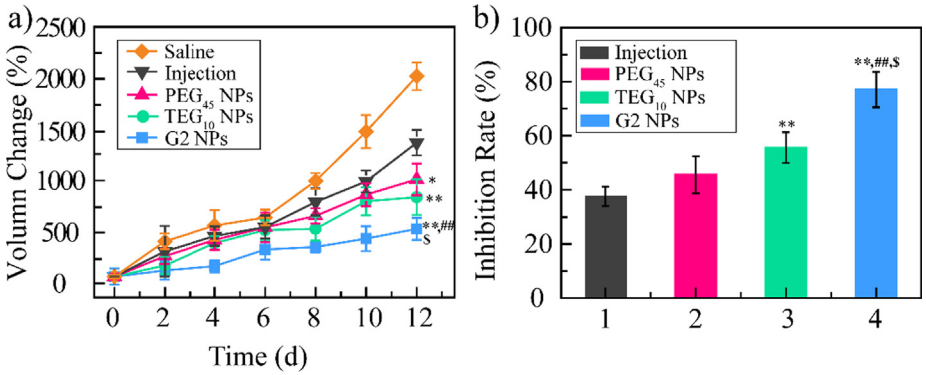

Fig. 6. *In vivo* tumor growth inhibition of HCPT nanoparticles. Tumor volume change curves (a) and tumor inhibition rate (b) (n = 10). Six consecutive doses were given (marked by arrows). $^{*}p < 0.05$, $^{**}p < 0.01$, *vs.* HCPT injection; $^{\#\#}p < 0.01$, G2 NPs *vs.* HCPT/PEG_{45} NPs; $^{\$}p < 0.05$, G2 NPs *vs.* HCPT/$TEG_{10}$ NPs.

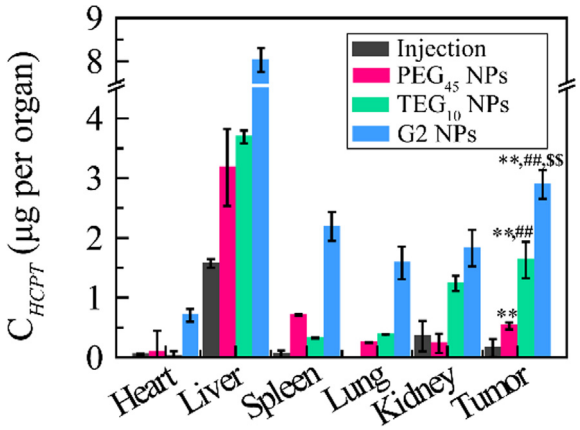

Fig. 7. HCPT biodistribution in BALB/c mice bearing tumors (n = 10) determined by HPLC. $^{**}p < 0.01$ *vs.* HCPT injection; $^{\#\#}p < 0.01$ *vs.* HCPT/PEG_{45} NPs; $^{\$\$}p < 0.01$, *vs.* HCPT/$TEG_{10}$ NPs.

effect of reticuloendothelial system (RES) [50].

3.7. Toxicity evaluation

The body weight of each mouse was monitored every two days to evaluate the systemic toxicity of these nanoparticles. During the whole experimental procedure, no mice dead and all mice presented normal status, meanwhile, the body weight was increased. As shown in Fig. 8, the mice treated with all HCPT NPs grew at approximately 5–10% of their initial weight, and no significant difference was shown between nanoparticles groups and normal saline group ($p > 0.05$), besides, HCPT NPs groups existed a higher weight increase than that of HCPT injection group. Based on these results, it seemed that HCPT NPs presented a negligible systemic toxicity.

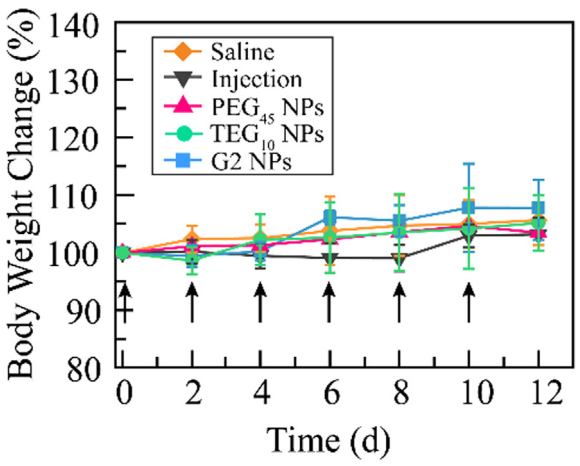

Fig. 8. The body weight change curves. For each animal, six consecutive doses were given (marked by arrows). Data represent mean ± SD (n = 10).

Due to the high accumulation in RES system, such as liver and kidney, it was necessary to research *in vivo* toxicity of HCPT NPs [51]. Therefore, the hepatic/renal function markers were measured, including alanine amino transferanse (ALT), aspartate amino transferase (AST), blood urea nitrogen (BUN), and creatinine (CRE). HCPT NPs showed no significant difference comparing with the other two groups ($p > 0.05$) (Table 2), including saline group and injection group. These results indicated that HCPT NPs presented no obvious hepatic or renal toxicity, although showing high accumulation in liver and kidney.

4. Conclusions

To evaluate the architecture effects of nanocarriers on antitumor efficacy, in this study, linear PEG (PEG_{45}), brush poly(triethylene glycol) (TEG_{10}), and oligo(ethylene glycol) dendron (G2) were utilized as nanocarriers to prepare 10-hydroxycamptothecin (HCPT) nanoparticles. All of these HCPT NPs showed the similar drug-loading content of approximately 60%, zeta potential of approximately −13 to −16 mV, and good stability in 5% glucose solution and plasma. However, it was found that the particle sizes, release profiles, and antitumor efficacies of HCPT NPs were related with the architecture of ethylene glycols. The particle size was 240, 191, and 173 nm for PEG_{45} NPs, TEG_{10} NPs, and G2 NPs respectively, and the sustained release was elongated from 5 to 9 days. The *in vitro* and *in vivo* antitumor efficacies of HCPT NPs were dependent with the branched degree of nanocarriers, G2 NPs existed the best antitumor efficacy, *in vitro* cytotoxicity was enhanced10.1-fold and 6.5-fold than PEG_{45} NPs and TEG_{10} NPs, the tumor inhibition rate *in vivo* was promoted 1.7-fold and 1.4-fold than PEG_{45} NPs and TEG_{10} NPs, due to the high biodistribution of G2 NPs in tumor tissue. In summary, this study demonstrated the insights that the architecture of nanocarriers could influence the antitumor activity, and these insights formulate rules for engineering NPs for cancer therapy.

Table 2
Plasma biochemical levels of 4T1 bearing BALB/c mice.

Sample	ALT (IU L^{-1})	AST (IU L^{-1})	CRE (μmol L^{-1})	BUN (mmol L^{-1})
Saline	11.22	9.45	17.39	4.12
Injection	10.49	11.03	12.29	3.97
PEG_{45} NPs	12.46	20.09	1.06	3.8
TEG_{10} NPs	10.25	29.16	41.91	4.91
G2 NPs	7.66	16.82	15.73	3.99

Acknowledgments

This work is financially supported by CAMS Innovation Fund for Medical Sciences (CIFMS, no. 2017-I2M-1-013), CAMS Innovation Fund for Medical Sciences (CIFMS, no. 2016-I2M-1-012), National Natural Science Foundation of China (no. 81573622), National Natural Science Foundation of China (no. U1401223). and the Program for Guangdong YangFan Introducing Innovative and Enterpreneurial Teams (no. 2017YT05S029)

Notes

The authors declare no competing financial interest.

References

[1] S. Mura, J. Nicolas, P. Couvreur, Stimuli-responsive nanocarriers for drug delivery, Nat. Mater. 12 (2013) 991–1003.
[2] J.-W. Yoo, D.J. Irvine, D.E. Discher, S. Mitragotri, Bio-inspired, bioengineered and biomimetic drug delivery carriers, Nat. Rev. Drug Discov. 10 (2011) 521–535.
[3] T. Doane, C. Burda, Nanoparticle mediated non-covalent drug delivery, Adv. Drug Deliv. Rev. 65 (2013) 607–621.
[4] M. Kanapathipillai, A. Brock, D.E. Ingber, Nanoparticle targeting of anti-cancer drugs that alter intracellular signaling or influence the tumor microenvironment, Adv. Drug Deliv. Rev. 79–80 (2014) 107–118.
[5] S.-Y. Qin, A.-Q. Zhang, S.-X. Cheng, L. Rong, X.-Z. Zhang, Drug self-delivery systems for cancer therapy, Biomaterials 112 (2017) 234–247.
[6] P. Grossen, D. Witzigmann, S. Sieber, J. Huwyler, PEG-PCL-based nanomedicines: a biodegradable drug delivery system and its application, J. Contr. Release 260 (2017) 46–60.
[7] K. Seidi, H.A. Neubauer, R. Moriggl, R. Jahanban-Esfahlan, T. Javaheri, Tumor target amplification: implications for nano drug delivery systems, J. Contr. Release 275 (2018) 142–161.
[8] P.I. Chater, M.D. Wilcox, J.P. Pearson, Efficacy and safety concerns over the use of mucus modulating agents for drug delivery using nanoscale systems, Adv. Drug Deliv. Rev. 124 (2018) 184–192.
[9] E. Pérez-Herrero, A. Fernández-Medarde, Advanced targeted therapies in cancer: drug nanocarriers, the future of chemotherapy, Eur. J. Pharm. Biopharm. 93 (2015) 52–79.
[10] A. Kolate, D. Baradia, S. Patil, I. Vhora, G. Kore, A. Misra, PEG — a versatile conjugating ligand for drugs and drug delivery systems, J. Contr. Release 192 (2014) 67–81.
[11] J.-M. Rabanel, P. Hildgen, X. Banquy, Assessment of PEG on polymeric particles surface, a key step in drug carrier translation, J. Contr. Release 185 (2014) 71–87.
[12] K. Knop, R. Hoogenboom, D. Fischer, U.S. Schubert, Poly(ethylene glycol) in drug delivery: pros and cons as well as potential alternative, Angew. Chem. Int. Ed 49 (2010) 6288–6308.
[13] S.N.S. Alconcel, A.S. Baas, H.D. Maynard, FDA-approved poly(ethylene glycol)-protein conjugate drugs, Polym. Chem-UK 2 (2011) 1442–1448.
[14] S. Venkataraman, J.L. Hedrick, Z.Y. Ong, C. Yang, P.L.R. Ee, P.T. Hammond, Y.Y. Yang, The effects of polymeric nanostructure shape on drug delivery, Adv. Drug Deliv. Rev. 63 (2011) 1228–1246.
[15] K. Zhang, X. Tang, J. Zhang, W. Lu, X. Lin, Y. Zhang, B. Tian, H. Yang, H. He, PEG–PLGA copolymers: their structure and structure-influenced drug delivery applications, J. Contr. Release 183 (2014) 77–86.
[16] C. Garofalo, G. Capuano, R. Sottile, R. Tallerico, R. Adami, E. Reverchon, E. Carbone, L. Izzo, D. Pappalardo, Different Insight into amphiphilic PEG-PLA copolymers: influence of macromolecular architecture on the micelle formation and cellular uptake, Biomacromolecules 15 (2014) 403–415.
[17] J.-M. Rabanel, J. Faivre, S.F. Tehrani, A. Lalloz, P. Hildgen, X. Banquy, Effect of the polymer architecture on the structural and biophysical properties of PEG–PLA nanoparticles, ACS Appl. Mater. Inter. 7 (2015) 10374–10385.
[18] S. Venkataraman, J.L. Hedrick, Z. Yuinong, Chuanyang, P.L. Rachelee, P.T. Hammond, Y. Yanyang, The effects of polymeric nanostructure shape on drug delivery, Adv. Drug Deliv. Rev. 63 (2011) 1228–1246.
[19] A. Agarwala, Y. Lvova, R. Sawantbc, V. Torchilinbc, Stable nanocolloids of poorly soluble drugs with high drug content prepared using the combination of sonication and layer-by-layer technology, J. Contr. Release 128 (2008) 255–260.
[20] I.N. Kurniasih, J. Keilitz, R. Haag, Dendritic nanocarriers based on hyperbranched polymers, Chem. Soc. Rev. 44 (2015) 4145–4164.
[21] D. Peer, J.M. Karp, S. Hong, O.C. Farokhzad, R. Margalit, R. Langer, Nanocarriers as an emerging platform for cancer therapy, Nat. Nanotech. 2 (2007) 751–760.
[22] X. Li, A.N. Sun, Y.-J. Liu, W.-J. Zhang, N. Pang, S.-X. Cheng, X.-R. Qi, Amphiphilic dendrimer engineered nanocarrier systems for co-delivery of siRNA and paclitaxel to matrix metalloproteinase-rich tumors for synergistic therapy, NPG Asia Mater. 10 (2018) 238–254.
[23] S. Mignani, S.E. Kazzouli, M. Bousmina, J.-P. Majoral, Expand classical drug administration ways by emerging routes using dendrimer drug delivery systems: a concise overview, Adv. Drug Deliv. Rev. 65 (2013) 1316–1330.
[24] P. Kesharwani, K. Jain, N.K. Jain, Dendrimer as nanocarrier for drug delivery, Prog. Polym. Sci. 39 (2014) 268–307.
[25] E.R. Gillies, J.M.J. Fréchet, Dendrimers and dendritic polymers in drug delivery, Drug Discov. Today 10 (2005) 35–43.
[26] S. Zhang, H.-J. Sun, A.D. Hughes, R.-O. Moussodia, A. Bertin, Y. Chen, D.J. Pochan, P.A. Heiney, M.L. Klein, V. Percec, Self-assembly of amphiphilic Janus dendrimers into uniform onion-like dendrimersomes with predictable size and number of bilayers, Proc. Natl. Acad. Sci. USA 111 (2014) 9058–9063.
[27] L. Sun, X. Ma, C. Dong, B. Zhu, X. Zhu, NIR-responsive and lectin-binding doxorubicin-loaded nanomedicine from Janus-type dendritic PAMAM amphiphiles, Biomacromolecules 13 (2012) 3581–3591.
[28] W. Wu, W. Wang, J. Li, Star polymers: advances in biomedical applications, Prog. Polym. Sci. 46 (2015) 55–85.
[29] J. Wang, J. Sun, Q. Chen, Y. Gao, L. Li, H. Li, D. Leng, Y. Wang, Y. Sun, Y. Jing, S. Wang, Z. He, Star-shape copolymer of lysine-linked di-tocopherol polyethylene glycol 2000 succinate for doxorubicin delivery with reversal of multidrug resistance, Biomaterials 33 (2012) 6877–6888.
[30] I. Gitsov, Hybrid linear dendritic macromolecules: from synthesis to applications, J. Polym. Sci. Polym. Chem. 46 (2008) 5295–5314.
[31] E. Mohammadifar, A.N. Kharat, M. Adeli, Polyamidoamine and polyglycerol; their linear, dendritic and linear–dendritic architectures as anticancer drug delivery systems, J. Mater. Chem. B 3 (2015) 3896–3921.
[32] R. Haag, F. Kratz, Polymer therapeutics: concepts and applications, Angew. Chem. Int. Ed. 45 (2006) 1198–1215.
[33] A. Ardana, A.K. Whittaker, K.J. Thurecht, PEG-based hyperbranched polymer theranostics: optimizing chemistries for improved bioconjugation, Macromolecules 47 (2014) 5211–5219.
[34] C.C. Lee, J.A. Mackay, J.M.J. Fréchet, F.C. Szoka, Designing dendrimers for biological applications, Nat. Biotechnol. 23 (2005) 1517–1526.
[35] M. Ahmed, R. Narain, The effect of molecular weight, compositions and lectin type on the properties of hyperbranched glycopolymers as non-viral gene delivery systems, Biomaterials 33 (2012) 3990–4001.
[36] L. Zhou, X. Qu, Y. Guo, M. Wang, B. Lei, P.X. Ma, Branched glycerol-based copolymer with ultrahigh p65 siRNA delivery efficiency for enhanced cancer therapy, ACS Appl. Mater. Inter. 10 (2018) 4471–4480.
[37] W. She, D. Pan, K. Luo, B. He, G. Cheng, C. Zhang, Z. Gu, PEGylated dendrimer-doxorubicin cojugates as pH-sensitive drug delivery systems: synthesis and in vitro characterization, J. Biomed. Nanotechnol. 11 (2015) 964–978.
[38] X. Li, E. Munenobutakashima, A. Yuba, K. Harada, Kono, PEGylated PAMAM dendrimer–doxorubicin conjugate-hybridized gold nanorod for combined photothermal-chemotherapy, Biomaterials 35 (2014) 6576–6584.
[39] J.A. Johnson, Y.Y. Lu, A.O. Burts, Y.-H. Lim, M.G. Finn, J.T. Koberstein, N.J. Turro, D.A. Tirrell, R.H. Grubbs, Core-clickable PEG-branch-azide bivalent-bottle-brush polymers by ROMP: grafting-through and clicking-to, J. Am. Chem. Soc. 133 (2011) 559–566.
[40] Y. Guo, C. Hao, X. Wang, Y. Zhao, M. Han, M. Wang, X. Wang, Well-defined podophyllotoxin polyprodrug brushes: preparation via RAFT polymerization and evaluation as drug carriers, Polym. Chem.-UK 8 (2017) 901–909.
[41] Y. Guo, Y. Zhao, J. Zhao, M. Han, A. Zhang, X. Wang, Codendrimer from polyamidoamine (PAMAM) and oligoethylene dendron as a thermosensitive drug carrier, Bioconjugate Chem. 25 (2014) 24–31.
[42] Y. Guo, Y. Zhao, T. Wang, R. Li, M. Han, Z. Dong, C. Zhu, X. Wang, Hydroxycamptothecin nanorods prepared by fluorescently labeled oligoethylene glycols (OEG) codendrimer: antitumor efficacy *in vitro* and *in vivo*, Bioconjugate Chem. 28 (2017) 390–399.
[43] Y. Guo, S. Zhao, H. Qiu, T. Wang, Y. Zhao, M. Han, Z. Dong, X. Wang, Shape of nanoparticles as a design parameter to improve docetaxel antitumor efficacy, Bioconjugate Chem. 29 (2018) 1302–1311.
[44] W. Li, X. Zhang, X. Hao, J. Jie, B. Tian, X. Zhang, Shape design of high drug payload nanoparticles for more effective cancer therapy, Chem. Commun. 49 (2013) 10989–10991.
[45] F. Xiong, J. Tian, K. Hu, X. Zheng, J. Sun, C. Yan, J. Yao, L. Song, Y. Zhang, N. Gu, Superparamagnetic anisotropic nano-assemblies with longer blood circulation in vivo: a highly efficient drug delivery carrier for leukemia therapy, Nanoscale 8 (2016) 17085–17089.
[46] X. Xu, W. Ho, X. Zhang, N. Bertrand, O. Farokhzad, Cancer nanomedicine: from targeted delivery to combination therapy, Trends Mol. Med. 21 (2015) 223–232.
[47] H. Maeda, Toward a full understanding of the EPR effect in primary and metastatic tumors as well as issues related to its heterogeneity, Adv. Drug Deliv. Rev. 91 (2015) 3–6.
[48] H. Kobayashi, R. Watanabe, P.L. Choyke, Improving conventional enhanced permeability and retention (EPR) effects; what is the appropriate target? Theranostics 4 (2014) 81–89.
[49] M. Xu, J. Qian, A. Suo, N. Cui, Y. Yao, W. Xu, T. Liua, H. Wanga, Co-delivery of doxorubicin and P-glycoprotein siRNA by multifunctional triblock copolymers for enhanced anticancer efficacy in breast cancer cells, J. Mater. Chem. B 3 (2015) 2215–2228.
[50] S. Sharifi, S. Behzadi, S. Laurent, M. Laird Forrest, P. Stroeve, M. Mahmoudi, Toxicity of nanomaterials, Chem. Soc. Rev. 41 (2012) 2323–2343.
[51] I. Khan, K. Saeed, I. Khan, Nanoparticles: Properties, applications and toxicities, Arab. J. Chem. (2017), https://doi.org/10.1016/j.arabjc.2017.05.011.